SUPPORTING APPENDIX

In the following, we give additional figures and examples, as well as the explicit `matlab` codes used in the numerical computations.

STRUCTURAL KINETIC MODELING

Our approach is based on an alternative parametric representation of the Jacobian matrix $\mathbf{J}$ of a metabolic system,

$$\mathbf{J_x} = \mathbf{\Lambda}\, \boldsymbol{\theta}^{\boldsymbol{\mu}}_{\mathbf{x}} \;, \tag{1}$$

where $\mathbf{\Lambda}$ is specified by the stoichiometric matrix and the (usually experimentally observed) operating point, and $\boldsymbol{\theta}^{\boldsymbol{\mu}}_{\mathbf{x}}$ denotes the matrix of normalized saturation parameters.
The transformation results from rewriting the original system in terms of new variables $\mathbf{x}$, such that $x_i = S_i/S_i^0$.

$$\frac{dS_i}{dt} = \sum_j N_{ij}\, \nu_j(\mathbf{S}) \quad \longrightarrow \quad \frac{dS_i}{dt} = \sum_j N_{ij} \underbrace{\frac{S_i^0}{S_i^0}}_{=1} \underbrace{\frac{\nu_j(\mathbf{S^0})}{\nu_j(\mathbf{S^0})}}_{=1} \nu_j(\mathbf{S}) \;. \tag{2}$$

Thus

$$\frac{1}{S_i^0}\frac{dS_i}{dt} = \sum_j \underbrace{N_{ij}\, \frac{\nu_j(\mathbf{S^0})}{S_i^0}}_{\Lambda_{ij}} \underbrace{\frac{\nu_j(\mathbf{S})}{\nu_j(\mathbf{S^0})}}_{\mu_j(\mathbf{x})} \;. \tag{3}$$

The Interpretation of the Saturation Parameter

The method crucially relies on the interpretation of the matrix $\boldsymbol{\theta}^{\boldsymbol{\mu}}_{\mathbf{x}}$ of normalized saturation parameters. We have to evaluate the partial derivatives of the normalized reaction rates $\boldsymbol{\mu}(\mathbf{x})$ with respect to the new normalized variables $\mathbf{x}$ at the point $\mathbf{x}^0 = \mathbf{1}$.
To prove the general case asserted in the manuscript,

$$\left.\frac{\partial \mu(x)}{\partial x}\right|_{\mathbf{x}^0=1} = n - \alpha m \quad \text{with} \quad \alpha \in [0,1]\,, \tag{4}$$

we write a given biochemical rate law $\nu(\mathbf{S},\mathbf{k})$ in the form

$$\nu(\mathbf{S},\mathbf{k}) = k_{\mathrm{v}} S^n / f_m(S,\mathbf{k})\,, \tag{5}$$

where S denotes a single reactant and the dependence on all other reactants has been absorbed into the parameters k_{v} and $\boldsymbol{k}$.
The function $f_m(S,\mathbf{k})$ denotes a polynomial of order m in S with positive coefficients $k_l \geq 0$ (1).

$$f_m(S,\mathbf{k}) = \sum_{l=0}^{m} k_l S^l \qquad \text{and} \quad k_l \geq 0\ \forall l = 0,\ldots,m \quad \text{with} \quad k_0 > 0\,. \tag{6}$$

Note that for $n = 0$, the equations also includes the case of product inhibition[†].

Applying the normalization transformation of Eq. **2** on the single reactant S and using the variable substitution $S \to xS^0$, we obtain

$$\mu(x) = \frac{\nu(S,\mathbf{k})}{\nu(S^0,\mathbf{k})} = x^n \frac{f_m(S^0)}{f_m(S^0 x)}\,. \tag{7}$$

The obtain the partial derivative at $x^0 = 1$, we write

$$\theta^{\mu}_{x} = \left.\frac{\partial \mu(x)}{\partial x}\right|_{x^0=1} = n + \left.\frac{\partial}{\partial x}\frac{f_m(S^0)}{f_m(S^0 x)}\right|_{x^0=1} = n - \underbrace{\frac{1}{f_m(S^0)}\left.\frac{\partial f_m(S^0 x)}{\partial x}\right|_{x^0=1}}_{=\alpha m \quad \text{(to show)}}\,. \tag{8}$$

Evaluating the last term and factoring out m results in

$$\left.\frac{\partial f_m(S^0 x)}{\partial x}\right|_{x^0=1} = \left.\frac{\partial}{\partial x}\sum_{l=0}^{m} k_l (S^0)^l x^l\right|_{x^0=1} = m \sum_{l=1}^{m} \frac{l}{m}\, k_l (S^0)^l\,. \tag{9}$$

Note that $\frac{l}{m} \leq 1$ for all $l = 0,\ldots,m$.
Resuming with the evaluation of Eq. **8** above, we thus obtain

$$\theta^{\mu}_{x} = n - m \underbrace{\frac{\sum_{l=1}^{m} \frac{l}{m} k_l (S^0)^l}{f_m(S^0)}}_{:=\alpha}\,. \tag{10}$$

[†]We require $k_0 > 0$, otherwise one S can be factored out and the order of the polynomial decreases. Note that n does not necessarily have to be positive or integer.

Using the definition

$$\alpha := \frac{\sum_{l=1}^{m} \frac{l}{m} k_l (S^0)^l}{f_m(S^0)} = \frac{\sum_{l=1}^{m} \frac{l}{m} k_l (S^0)^l}{\sum_{l=0}^{m} k_l (S^0)^l} , \tag{11}$$

we have to demonstrate that $\alpha \in [0, 1]$.
Since all coefficients in the polynomial are positve $k_l \geq 0$ and $k_l \geq \frac{l}{m} k_l$ for all k_l and $l = 0, \ldots, m$ the demoniator in Eq. **11** is indeed always larger or equal to the numerator. Thus finally

$$\theta_x^\mu = n - m \frac{\sum_{l=1}^{m} \frac{l}{m} k_l (S^0)^l}{\sum_{l=0}^{m} k_l (S^0)^l} = n - m\,\alpha \qquad \text{with} \quad \alpha \in [0, 1] . \tag{12}$$

For a vanishing steady-state substrate concentration $\lim S^0 \to 0$, we obtain

$$\lim_{S^0 \to 0} \alpha = 0 . \tag{13}$$

For very large steady-state substrate concentrations $\lim S^0 \to \infty$, the dominating terms in Eq. **11** are those with the highest exponent, thus

$$\lim_{S^0 \to \infty} \alpha = 1 . \tag{14}$$

Thus, if θ_x^μ is restricted to the appropriate interval, specified by the exponents of the rate law, it indeed covers all possible values of the (normalized) partial derivative at the steady-state concentration S^0. Note that the limiting cases $\lim_{S^0 \to 0} \alpha = 0$ and $\lim_{S^0 \to \infty} \alpha = 1$ do not depend on the parameters k_v and $\boldsymbol{k}$ of the original rate equation.

Some Examples of Biochemical Rate Equations

In addition to the examples given in *Materials and Methods*, we illustrate the normalization transformation and the interpretation of the saturation parameters using several commonly used biochemical rate laws.
Starting with the basic Michaelis-Menten rate law $\nu(S) = v_{\max} S/(K_{\mathrm{M}} + S)$, we obtain

$$\mu(x) = x\,\frac{K_M + S^0}{K_M + x\,S^0} \qquad \Rightarrow \qquad \theta^{\mu}_{x} = \frac{\partial \mu(x)}{\partial x} = \frac{1}{1 + S^0/K_M} \;\in [0,1]\;.$$

Clearly, the partial derivative $\theta^{\mu}_{x} \in [0,1]$ measures the degree of saturation or, likewise, the 'effective kinetic order' (in the nomenclature of the power-law formalism) of the reaction at the steady state S^0. This is illustrated in Fig. 8.

Michaelis-Menten kinetics with competitive inhibition:
Including 'competitive inhibition' by a metabolite I, results in

$$\nu(S,I) = \frac{v_{\max}\,S/K_M}{1 + S/K_{\mathrm{M}} + I/K_I} \qquad \Rightarrow \qquad \mu(x_S, x_I) = x_S\,\frac{1 + S^0/K_M + I^0/K_I}{1 + x_S\,S^0/K_M + x_I I^0/K_I}\;.$$

The normalized partial derivative with respect to the normalized variable x_S is thus

$$\theta^{\mu}_{x_S} = 1 - \frac{S^0/K_M}{1 + S^0/K_M + I^0/K_I} \;\in [0,1]\;,$$

with the limiting cases $\theta^{\mu}_{x_S} = 1$ for $S^0 \to 0$ (linear regime) and $\theta^{\mu}_{x_S} = 0$ for $S^0 \to \infty$ (full saturation). For the inhibitor I, we obtain

$$\theta^{\mu}_{x_I} = \frac{-I^0/K_I}{1 + S^0/K_M + I^0/K_I} \;\in [0,-1]\;,$$

with the limiting cases $\theta^{\mu}_{x_I} = -1$ for $I^0 \to \infty$ and $\theta^{\mu}_{x_I} = 0$ for $I^0 \to 0$. Note that the saturation parameter again covers the full interval, irrespective of the values of S^0 and K_M.

Additional noncompetitive inhibition:
Similar, when an additional 'noncompetitive inhibition' by a metabolite I_2 is included

$$\nu(S, I_1, I_2) = \frac{v_{\max}\,S/K_M}{(1 + S/K_{\mathrm{M}} + I_1/K_{I_1})\,(1 + I_2/K_{I_2})}\;.$$

The normalized rate equation with respect to the variables x_S, x_{I1}, and x_{I2} at the steady state S^0, I_1^0, and I_2^0 is

$$\mu(x_S, x_{I1}, x_{I2}) = x_S\,\frac{(1 + S^0/K_{\mathrm{M}} + I_1^0/K_{I_1})\,(1 + I_2^0/K_{I_2})}{(1 + x_S S^0/K_{\mathrm{M}} + x_{I1} I_1^0/K_{I_1})\,(1 + x_{I2} I_2^0/K_{I_2})}\;.$$

In this case, the saturation parameters with respect to x_S and x_{I1} remain unchanged.
For the partial derivative $\theta^{\mu}_{x_{I2}}$ with respect to x_{I2} we obtain

$$\theta^{\mu}_{x_{I2}} = \frac{-I_2^0/K_{I_2}}{1 + I_2^0/K_{I_2}} \;\in [0,-1]\;. \tag{15}$$

Note that $\theta^{\mu}_{x_I 2}$ does not depend on the values of S^0 and I_1^0.

Note: For any rate equation consisting of several multiplicative functions, the normalized saturation parameter with respect to a reactant S depends only on those functions in which S appears.

A specific example: The fructokinase in sugar cane

An explicit example of a biochemical rate law is the random-order bireactant kinetic, here including inhibition by ADP and fructose, which was used previously to model the fructokinase (FK) in sugar cane (2).

$$\nu_{\mathrm{FK}} = \frac{v_{\max}}{1+\frac{[\mathrm{Fruc}]}{K_I}} \cdot \frac{\frac{[\mathrm{Fruc}]}{K_F}\frac{[\mathrm{ATP}]}{K_{ATP}}}{1+\frac{[\mathrm{Fruc}]}{K_F}+\frac{[\mathrm{Fruc}]}{K_F}\frac{[\mathrm{ATP}]}{K_{ATP}}+\frac{[\mathrm{ADP}]}{K_{ADP}}} .$$

For the saturation parameters with respect to ATP and ADP, we obtain

$$\theta^{\mathrm{FK}}_{\mathrm{ATP}} \in [0,1] \qquad \text{and} \qquad \theta^{\mathrm{FK}}_{\mathrm{ADP}} \in [0,-1] .$$

More interesting is the saturation parameter with respect to fructose

$$\theta^{\mathrm{FK}}_{\mathrm{Fruc}} = 1 - \underbrace{\frac{\frac{[\mathrm{Fruc}]^0}{K_I}}{1+\frac{[\mathrm{Fruc}]^0}{K_I}}}_{\alpha_I\in[0,1]} - \underbrace{\frac{\frac{[\mathrm{Fruc}]^0}{K_F}+\frac{[\mathrm{Fruc}]^0}{K_F}\frac{[\mathrm{ATP}]^0}{K_{ATP}}}{1+\frac{[\mathrm{Fruc}]^0}{K_F}+\frac{[\mathrm{Fruc}]^0}{K_F}\frac{[\mathrm{ATP}]^0}{K_{ATP}}+\frac{[\mathrm{ADP}]^0}{K_{ADP}}}}_{\alpha_F\in[0,1]} \in [-1,1] .$$

In terms of the general case given by Eq. **4** the exponents are $n=1$ and $m=2$, thus $\theta^{\mathrm{FK}}_{\mathrm{Fruc}} = 1-2\alpha$ with $\alpha \in [0,1]$. Thus, indeed $\theta^{\mathrm{FK}}_{\mathrm{Fruc}} \in [-1,1]$.

Note: The Jacobian is fully defined by the saturation parameter $\theta^{\mathrm{FK}}_{\mathrm{Fruc}} \in [-1,1]$. However, two independent Michaelis constants, K_I and K_F, are needed to determine this value in the explicit rate law. However, for the linear properties of the system, as well as the occurence of certain bifurcations, only the combination of both Michaelis constants is relevant. ($\theta^{\mathrm{FK}}_{\mathrm{Fruc}} = 1-\alpha_I-\alpha_F$ with $\alpha_I \in [0,1]$ and $\alpha_F \in [0,1]$.) In this sense, our approach allows to identify related parameters in explicit equations.

A specific example: The Rubisco reaction in models of the Calvin cycle

Another example is the rate equation used in Ref. (3) to model the Rubisco reaction in the photosynthetic Calvin cycle.

$$\nu_{\mathrm{Rubisco}} = \frac{v_{\max}\frac{[\mathrm{RuBP}]}{K_1}}{1+\frac{[\mathrm{RuBP}]}{K_1}+\frac{[\mathrm{PGA}]}{K_2}+\frac{[\mathrm{FBP}]}{K_3}+\frac{[\mathrm{SBP}]}{K_4}+\frac{[\mathrm{Pi}]}{K_5}+\frac{[\mathrm{NADPH}]}{K_6}} .$$

Obviously, the rate equation follows the general case given by Eq. **4**, thus $\theta^{\mathrm{Rubisco}}_{\mathrm{RuBP}} \in [0,1]$ and $\theta^{\mathrm{Rubisco}}_{\mathrm{x}} \in [0,-1]$ for the dependence on all other reactants X.

Sigmoidal kinetics: The Hill equation

An example of sigmoidal kinetics is given by the 'Hill equation' (1),

$$\nu_{\mathrm{Hill}}(S) = \frac{v_{\max}\,(S/K_S)^n}{1+(S/K_S)^n} \qquad \Rightarrow \qquad \mu_{\mathrm{Hill}}(x) = x^n\,\frac{1+(S^0/K_S)^n}{1+(x\,S^0/K_S)^n} ,$$

where $n \geq 1$ denotes the Hill coefficient. Thus

$$\theta_x^{\text{Hill}} = n \cdot \frac{1}{1 + (S^0/K_S)^n} \in [0, n] \ .$$

The saturation parameter $\theta_x^{\text{Hill}} \in [0, n]$ is monotonically decreasing for increasing saturation, see Fig. 9.

Note: Despite its definition as a partial derivative, the parameter θ_x^{μ} does not measure the slope of the rate equation[‡]. As can be verified for the Hill equation, θ_x^{Hill} decreases monotonically for increasing saturation. Hence the term saturation parameter.

A specific example: Inhibition of the phosphofructokinase by ATP

A heuristic variation of the Hill equation was used in Ref. (4) to model the combined PFK-HK reaction (See reaction ν_1 in Fig. 2.) The reaction includes inhibition by its substrate ATP.

$$\nu_{\text{PFK-HK}} = k\,[\text{Glc}][\text{ATP}]\,f([\text{ATP}]) \quad \text{with} \quad f([\text{ATP}]) = \left[1 + \left(\frac{[\text{ATP}]}{K_I}\right)^n\right]^{-1} \ . \tag{16}$$

With respect to ATP, we have linear activation due to its effect as a substrate and inhibition with a positive exponent (Hill coefficient) n. According to the discussion above, we thus expect for the corresponding saturation parameter $\theta_{\text{ATP}}^{\text{PFK-HK}} = 1 - \xi$, with $\xi \in [0, n]$. Indeed, in terms of the normalized variables g (glucose) and a (ATP)

$$\mu_{\text{PFK-HK}}(g, a) = g\,a\,\frac{1 + \left(\frac{[\text{ATP}]^0}{K_I}\right)^n}{1 + \left(\frac{a[\text{ATP}]^0}{K_I}\right)^n} \qquad \Rightarrow \qquad \theta_{\text{ATP}}^{\text{PFK-HK}} = 1 - \underbrace{n\,\frac{\left(\frac{[\text{ATP}]^0}{K_I}\right)^n}{1 + \left(\frac{[\text{ATP}]^0}{K_I}\right)^n}}_{\xi \in [0,n]} \ . \tag{17}$$

This example also demonstrates that the exponent n is only relevant in combination with the saturation of the respective reaction, as determined by the Michaelis constant K_I. We write $\xi = \alpha n$ with $\alpha \in [0, 1]$. Only the product of both terms appears within the Jacobian. A small exponent (small Hill coefficient) can be compensated by a high saturation and vice versa. Often this allows one to specify a minimal exponent for which certain bifurcations can be expected.

Note: For our reasoning to hold, forward and backward terms in reversible rate equations have to be treated separately. As in most cases the denominator is identical, this does not give rise to additional saturation parameters. Consider the case of a reversible bireactant rate equation of the form

$$\text{A} + \text{B} \leftrightarrow \text{P} + \text{Q} \qquad \text{with} \qquad \nu = v_{\max}\frac{AB - PQ/K_{eq}}{f(A, B, P, Q)} \ . \tag{18}$$

Treating both terms in $\nu = \nu_+ - \nu_-$ separately, result in the normalized rates

$$\mu_+ = ab\frac{f(A^0, B^0, P^0, Q^0)}{f(aA^0, bB^0, pP^0, qQ^0)} \qquad \text{and} \qquad \mu_- = pq\frac{f(A^0, B^0, P^0, Q^0)}{f(aA^0, bB^0, pP^0, qQ^0)} \ . \tag{19}$$

[‡]However, θ_x^{μ} measures the slope of the rate law in a double logarithmic plot.

Thus, obviously, $\theta_a^{\mu+} = 1 - \alpha$ and $\theta_a^{\mu-} = \alpha$, with α depending on the function $f(A, B, P, Q)$. However, within the matrix $\mathbf{\Lambda}$ one additional parameter arises, corresponding to the cycling flux.

In the following, our analysis is entirely based on an interpretation of the saturation parameters and does not make any use of the explicit functional form of the rate equations.

An Illustrative Example

Though the hypothetical pathway given in Fig. 1 serves only illustrative purposes, we provide a brief analysis of its dynamical capabilities.

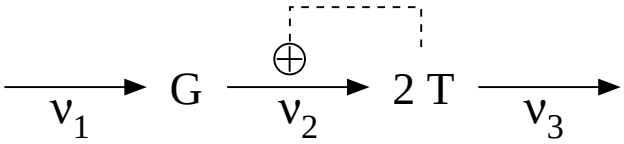

Following the model proposed in Ref. (5), one unit of glucose (G) is converted into two units of ATP (T), with ATP exerting a positive feedback on its own production.
We assume that the average concentrations G^0 and T^0 of both reactants have been determined experimentally. The stoichiometric matrix $\mathbf{N}$, with its associated null-space $\mathbf{K} = [1\ 1\ 2]^{\mathrm{T}}$, reveals that there is only one independent reaction rate $v_1 = c$. This information enables the construction of the matrix $\mathbf{\Lambda}$ and defines the operating point of the system (see main text for details).
The only free parameters at the observed operating point are thus the normalized degree of saturation $\theta^2_{\mathrm{G}} \in [0, 1]$ of ν_2 with respect to its substrate glucose (G) and the normalized degree of saturation $\theta^3_{\mathrm{T}} \in [0, 1]$ of ν_3 with respect to its substrate ATP (T). Furthermore , the feedback of ATP upon ν_2 is measured by $\theta^2_{\mathrm{T}} \in [0, n]$, where $n \geq 1$ denotes a positive integer. Given these parameters, we are in a position to investigate quantitatively the bifurcations inherent to structure of the Jacobian.
The two-dimensional pathway gives rise to a Hopf bifurcation, which indicates the emergence of sustained oscillations, independent from any further assumptions about the biochemical rate laws. Fig. 10 shows the bifurcation diagram of the system at the (assumed) experimentally observed operating point. The blue surface denotes the Hopf bifurcation, above which the steady state (G^0, T^0) loses its stability. As can be observed, with increasing saturation of the reactions (θ^2_{G} and $\theta^3_{\mathrm{T}} \to 0$) the oscillatory region increases in size, i.e., the Hopf bifurcation occurs for lower values of θ^2_{T}.
The red surface denotes the emergence of a pair of complex conjugate eigenvalues: in between the red and blue surfaces the system exhibits an oscillatory return to the asymptotically stable steady state.
The right plot in Fig. 10 shows a cut through the diagram at $\theta^2_{\mathrm{G}} = 1$ (linear dependence of ν_2 on its substrate G, no saturation), corresponding to the case studied by Bier *et al.* (5) using explicit differential equations. Inbetween both lines, the system exhibits an oscillatory return to the stable steady state.
Note that since the pathway only consists of two metabolites, bifurcations of higher codimensions, such as a double Hopf bifurcation, cannot arise.

Dynamics and Bifurcations

One of the foundations of our approach is the fact that knowledge of the Jacobian matrix alone is sufficient to deduce certain characteristic bifurcations of a metabolic system. In general, the stability of a steady state is lost either in a Hopf bifurcation (HO) or in a bifurcation of the saddle-node (SN) type, both of codimension-1. At an SN bifurcations a single zero eigenvalue of the Jacobian appears as the number or stability of steady states changes. Bifurcations of the SN type often indicate the presence of multiple steady states.

As the only other local codimension-1 bifurcation, a Hopf bifurcation occurs as a complex conjugate pair of eigenvalues crosses the imaginary axis towards positive real parts. This gives rise to (at least transient) oscillations as the stability of the steady state is lost. Note that it is not possible to distinguish between a sub- and supercritical Hopf bifurcation solely on basis of the Jacobian.

Of particular interest to reveal insights about the dynamical behavior of systems are also bifurcations of higher codimension, such as a Takens-Bogdanov (TB), a Gavrilov-Guckenheimer (GG), or a double Hopf (DH) bifurcation. Each of these local bifurcations of codimension-2 arises out of an interaction of two codimension-1 bifurcations and has important implications for the possible dynamical behavior. For instance, a TB bifurcation indicates the presence of a homoclinic bifurcation and therefore the possibility of spiking or bursting behavior. The presence of a GG bifurcation shows that complex (quasiperiodic or chaotic) dynamics exist generically in a certain parameter space. In the same way a DH bifurcation indicates the generic existence of a chaotic parameter region. For a more thorough mathematical description, see refs. (6) and (7).

THE GLYCOLYTIC PATHWAY

The first example within the main text is a medium-complexity representation of the anaerobic glycolytic pathway, adapted from earlier kinetic models (4, 8):

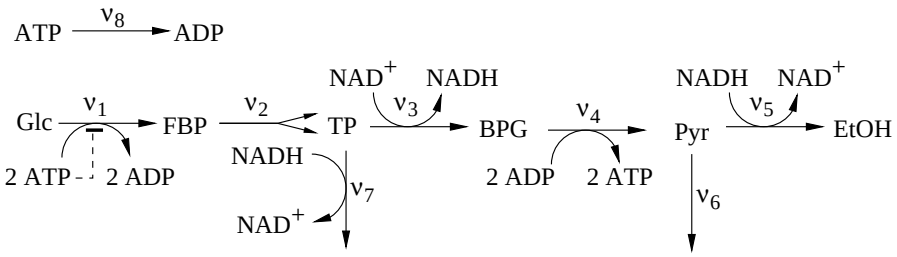

Metabolite abbreviations are as follows: Glucose (Glc), fructose-1,6-biphosphate (FBP), pool of triosephosphates (TP), 1,3-biphsophoglycerate (BPG), pool of pyruvate and acetaldehyde (Pyr), and ethanol (EtOH). Glc and EtOH are assumed to be the external source and sink, respectively.

The stoichiometric matrix $\boldsymbol{N}$ is as follows:

	ν_1	ν_2	ν_3	ν_4	ν_5	ν_6	ν_7	ν_8
FBP	+1	-1	0	0	0	0	0	0
TP	0	+2	-1	0	0	0	-1	0
BPG	0	0	+1	-1	0	0	0	0
Pyr/ACA	0	0	0	+1	-1	-1	0	0
ATP	-2	0	0	+2	0	0	0	-1
NADH	0	0	+1	0	-1	0	-1	0
NAD^+	0	0	-1	0	+1	0	+1	0
ADP	+2	0	0	-2	0	0	0	+1

The rank of the stoichiometric matrix is $\mathrm{rank}(\boldsymbol{N}) = 6$, corresponding to the 6 steady-state mass conservation constraints. Thus, all feasible steady-state flux vectors $\boldsymbol{\nu}(\boldsymbol{S^0})$ can be described by two basis vectors $\mathbf{k}_i$:

$$\boldsymbol{\nu}(\boldsymbol{S^0}) = \sum_{i=1}^{2} \mathbf{k}_i c_i = \begin{pmatrix} 1 \\ 1 \\ 1 \\ 1 \\ 0 \\ 1 \\ 1 \\ 0 \end{pmatrix} c_1 + \begin{pmatrix} 1 \\ 1 \\ 2 \\ 2 \\ 2 \\ 0 \\ 0 \\ 2 \end{pmatrix} c_2 \ . \tag{20}$$

The Choice of the Operating Point

To evaluate the structural kinetic model, we focus on a specific experimentally observed operating point of the system. However, in the case of sustained oscillations, the (in this case unstable) steady state cannot be observed directly. Within the main text, we thus approximate the operating point at which the system is to be evaluated by the average of the observed concentration and flux values, as reported in (4, 9):

average metabolite concentrations [mM]								**flux values [mM · min^{-1}]**	
FBP	**TP**	**BPG**	**Pyr**	**ATP**	**NADH**	**NAD**	**ADP**	$\mathbf{c_1}$	$\mathbf{c_2}$
5.1	0.12	0.0001	1.48	2.1	0.33	0.67	1.9	20.0	30.0

These values, together with the stoichiometric matrix $\mathbf{N}$, fully specify the matrix $\mathbf{\Lambda}$.

The approximation by the average quantities is justified by the assumption that in most cases the actual unstable state of the system is reasonably close to the average values. However, to ascertain that our result do not depend crucially on the exact knowledge of the operating point, we have to repeat the analysis, including variation of the assumed unstable steady state.
Fig. 11 exemplifies the small deviation between the actual unstable state and the average of the observed values, using an explicit model of the glycolytic pathway (parameters as in Fig. 3*d*). As we do not assume precise knowledge of the operating point, we allow for some variation around the average of the experimentally observed values, as depicted in Fig. 11*Right*.
Figure 12 repeats the analysis shown in Fig. 3, but including a relative 20% variation in each steady-state variable (choosen from a gaussian centered at the average observed values). As can be observed, the results do not depend crucially on the precise knowledge of the actual unstable steady state. The transition to (at least transient) oscillatory behavior is robust with respect to the assumed unstable state.

Note: A similar situation also arises in the evaluation of explicit kinetic models: Any explicit model will eventually result in a numerical simulation of a particular set of parameters, and it is far from certain, and indeed rather unlikely, that these are the exact parameters of the actual system. An appropriate way to account for this, though computationally demanding and only rarely done for explicit models, is to repeat the analysis for a large set of parameters in close vicinity of the original set of parameters (thus to ensure that the observed behavior indeed persists and is not an artifact of one particular set of parameters).

Note: A similar strategy can be adopted if large fluctuations of the experimentally observed concentrations are observed. In this case, it is appropriate not to focus only on one specific state, but to include the fluctuations into the evaluation of the system.

Note: While often the mean of the observed concentration values is indeed a reasonable approximation of the actual state, this must not always be the case. In particular, when the experimentally observed concentration values follow a strongly skewed distribution (such as a power law), the mean is no longer appropriate. In this case, the (vicinity of the) state at which the Jacobian is to be evaluated has to be chosen in accordance with the distribution of the experimentally observed concentration values.
Similar, one may refine the range of variation shown in Fig. 12 by including amplitude and covariance of the experimentally observed concentration values.

The Structural Kinetic Model

Second, the dependence of each reaction on the metabolites has to be specified as follows:

	FBP	TP	BPG	Pyr/ACA	ATP	NADH	NAD^+	ADP
ν_1	0	0	0	0	θ^1_{ATP}	0	0	0
ν_2	θ^2_{FBP}	0	0	0	0	0	0	0
ν_3	0	θ^3_{TP}	0	0	0	0	θ^3_{NAD}	0
ν_4	0	0	θ^4_{BPG}	0	0	0	0	θ^4_{ADP}
ν_5	0	0	0	θ^5_{Pyr}	0	θ^5_{NADH}	0	0
ν_6	0	0	0	θ^6_{Pyr}	0	0	0	0
ν_7	0	θ^7_{TP}	0	0	0	θ^7_{NADH}	0	0
ν_8	0	0	0	0	θ^8_{ATP}	0	0	0

For simplicity all reactions are irreversible and depend on their substrates only, resulting in 12 free saturation parameters. The dependence of ν_1 on ATP is given as $\theta^1_{\mathrm{ATP}} = 1 - \xi$ with $\xi \in [0, n]$.
To obtain an explicit representation of the matrix $\boldsymbol{\theta}^{\boldsymbol{\mu}}_{\mathbf{x}}$, we have to take into account the two conservation relations ATP+ADP = const. and NAD^+ + NADH = const. Using the definition $\beta_1 = [\mathrm{ATP}]^0/[\mathrm{ADP}]^0$ and $\beta_2 = [\mathrm{NADH}]^0/[\mathrm{NAD^+}]^0$, we obtain

$$\boldsymbol{\theta}^{\boldsymbol{\mu}}_{\mathbf{x}} = \begin{pmatrix} 0 & 0 & 0 & 0 & 1-\xi & 0 \\ \theta^2_{\mathrm{FBP}} & 0 & 0 & 0 & 0 & 0 \\ 0 & \theta^3_{\mathrm{TP}} & 0 & 0 & 0 & -\beta_2 \cdot \theta^3_{\mathrm{NAD}} \\ 0 & 0 & \theta^4_{\mathrm{BPG}} & 0 & -\beta_1 \cdot \theta^4_{\mathrm{ADP}} & 0 \\ 0 & 0 & 0 & \theta^5_{\mathrm{Pyr}} & 0 & \theta^5_{\mathrm{NADH}} \\ 0 & 0 & 0 & \theta^6_{\mathrm{Pyr}} & 0 & 0 \\ 0 & \theta^7_{\mathrm{TP}} & 0 & 0 & 0 & \theta^7_{\mathrm{NADH}} \\ 0 & 0 & 0 & 0 & \theta^8_{\mathrm{ATP}} & 0 \end{pmatrix} .$$

Note: Generally, conserved pools of metabolites reduce the number of independent variables. Consider the case $S_1 + S_2 = const.$, then

$$x_1 + x_2 \frac{S_2^0}{S_1^0} = const. \tag{21}$$

The dependence of each normalized reaction rate μ on x_1 can thus be written in terms of x_2 and the partial derivative with respect to x_2 transforms into

$$\theta^{\mu}_{x_2} \quad \longrightarrow \quad \theta^{\mu}_{x_2} - \frac{S_2^0}{S_1^0}\theta^{\mu}_{x_1} \ . \tag{22}$$

Similar for the more general case $\sum_i m_i S_i = const.$, where m_i denotes a constant integer. Then

$$x_k = const - \sum_{i \neq k} \frac{m_i}{m_k} \frac{S_i^0}{S_k^0} x_i \ . \tag{23}$$

and the partial derivatives have to be replaced accordingly (see *The Photosynthetic Calvin Cycle* for an explicit example).

The Matlab Code

```
function [J] = GlycolysisJacobian
% The (schematic) function returns the normalized Jacobian
% of the model depicted in Fig. 2.

% The colum vector of metabolite concentrations
X0 = [FBP  TP  BPG Pyr ATP NADH NAD ADP]';

% The stoichiometric matrix
N=[ +1    -1    0    0    0    0    0    0 ;
     0    +2   -1    0    0    0   -1    0 ;
     0     0   +1   -1    0    0    0    0 ;
     0     0    0   +1   -1   -1    0    0 ;
    -2     0    0   +2    0    0    0   -1 ;
     0     0   +1    0   -1    0   -1    0 ;
     0     0   -1    0   +1    0   +1    0 ;
    +2     0    0   -2    0    0    0   +1 ];

% The null space of N
K =[1     1;
    1     1;
    1     2;
    1     2;
    0     2;
    1     0;
    1     0;
    0     2];

% The row vector of steady state fluxes
c1=20.0; c2=30.0; v=(K*[ c1 ; c2 ])';

% Define the matrix LAMBDA
N0=N(1:6,:);
LAMBDA=N0.*v(ones(6,1),:);
LAMBDA=LAMBDA./X0(1:6,ones(8,1));

% Construct the matrix of saturation coefficients
t;  % a vector containing the 11 nonzero elements of theta
xi; % A parameter specifying the feedback
b1 = ATP/ADP; b2 = NADH/NAD;

% The matrix theta
 theta = [   0       0     0    0     1-xi        0 ;
           t(1)      0     0    0        0        0 ;
             0     t(2)    0    0        0  -b2*t(3);
             0       0   t(4)   0  -b1*t(5)       0 ;
             0       0     0  t(6)       0      t(7);
             0       0     0  t(8)       0        0 ;
             0     t(9)    0    0        0     t(10);
             0       0     0    0     t(11)       0 ];

% The Jacobian matrix in terms of the normalized variables
J = LAMBDA*theta; % the scaled Jacobian
```

An Explicit Kinetic Model

To verify the dynamical behavior predicted by the Jacobian, we use an explicit kinetic model of the pathway (see Fig. 3).
Following the model of Wolf *et al.* (4), all rate equations are modeled as bilinear mass-action $\nu_i(\mathbf{S}) = k_i \prod S_i$. Only the combined PFK-HK reaction ν_1 contains a nonlinear saturable term (see above).

$$\nu_1 = k_1\,[\mathrm{Glc}][\mathrm{ATP}]\,f([\mathrm{ATP}]) \quad \text{with} \quad f([\mathrm{ATP}]) = \left[1 + \left(\frac{[\mathrm{ATP}]}{K_I}\right)^n\right]^{-1} . \tag{24}$$

The parameters are chosen such that the model reproduces the desired steady state $\mathbf{S^0}$. In particular, for the bilinear rate equations $k_i = v_i^0 / \prod S_i^0$. For the combined PFK-HK reaction, we have to specify the parameters k_1 and K_I, using

$$K_I = [\mathrm{ATP}]^0 \left(\frac{\xi}{n-\xi}\right)^{\frac{1}{n}} \qquad \text{and} \qquad k_1 = \frac{v_1^0}{[\mathrm{Glc}]^0[\mathrm{ATP}]^0}\frac{n}{\xi} , \tag{25}$$

with an exponent $n = 4$ (4). In this way, the explicit model is consistent with the structural kinetic model used in Fig. 3. All saturation parameters are $\theta_x^\mu = 1$, except $\theta^1_{\mathrm{ATP}} = 1 - \xi$ with $\xi \in [0, 4)$.

Note: Not all explicit kinetic models can reproduce all possible Jacobian matrices of the full structural kinetic model. For example, by using only bilinear rate equations all saturation parameters are restricted to the unit value. However, it is always possible to construct an explicit model that is consistent with a given Jacobian.

Analysis of the Structural Kinetic Model

In the following, we provide additional figures with respect to the analysis of the yeast glycolytic pathway depicted in Fig. 2.

Note: Similar to conventional modeling, all results of course depend on the initial (stoichiometric) definition of the model itself. Prior to the analysis it has to be specified whether certain reactions are to be included in the model, whether cofactors are considered explicitely or assumed constant, as well as which reactions are treated as reversible or irreversible. As with explicit kinetic modeling, based on differential equations, these decisions will affect the properties of the system. In our case, all results relate to the medium complexity representation of the pathway shown in Fig. 2.

As one of its primary features, the method described in the main text allows one to explore rather large regions of the parameter space and serves to identify crucial reaction steps that predominantly contribute to the stability of the system. To this end, the saturation parameters $\theta_x^\mu \in [0, 1]$ are sampled repeatedly from a given (in this case uniform) distribution.
Relating to Fig. 4, we look for reaction parameters that exhibit a strong correlation with the stability of the system (see text for details). The correlation coefficient between the stability, measured by the largest real part of the eigenvalues of the Jacobian, and the 11 saturation parameters is estimated as:

θ^2_{FBP}	θ^3_{TP}	$\theta^3_{\mathrm{NAD+}}$	θ^4_{BPG}	θ^4_{ADP}	θ^5_{Pyr}	θ^5_{NADH}	θ^6_{Pyr}	θ^7_{TP}	θ^7_{NADH}	θ^8_{ATP}
0.40	0.27	0.03	0.00	-0.00	0.28	0.01	-0.23	-0.20	-0.03	-0.55

.

An alternative, and maybe more appropriate way to assess the impact of each reaction parameter upon the stability of the system, is to select for instances of the Jacobian that result in a stable operating point. Subsequently, the distribution of parameters of these Jacobians is compared to the initial (here: uniform) distribution of the parameters. The approach is visualized in Fig. 13. Importantly, in this way we only rely on a comparision of distributions and the results do not depend on the shape of the initial distribution.
Fig. 14 repeats the analysis for several other saturation parameters. As can be observed, in some cases the resulting distribution is markedly changed, indicating that these saturation parameters contribute predominantly to the stability of the system.

Note: $\lambda_R^{\max} < 0$ implies stability of the operating point and is a necessary condition to actually observe the system at a steady state with the experimentally given metabolite concentrations and flux values. However, $\lambda_R^{\max} < 0$ does not imply global stability of the operating point, i.e., there might be coexisting attractors, such that for a large enough perturbations the system will not return to the operating point.

THE PHOTOSYNTHETIC CALVIN CYCLE

Displayed below is the reaction scheme of the photosynthetic Calvin cycle, adapted from earlier kinetic models (3, 10). The systems consists of 18 metabolites, subject to two conservation relations, and 20 reactions, including 3 export reactions, starch synthesis, and regeneration of ATP. The rank of the stoichiometric matrix is $\mathrm{rank}(\mathbf{N}) = 16$, leaving 4 independent steady-state reaction rates. The model describes chloroplast metabolism with triosephosphate (TP) export and starch production as main output processes. For details, see the the original publications.

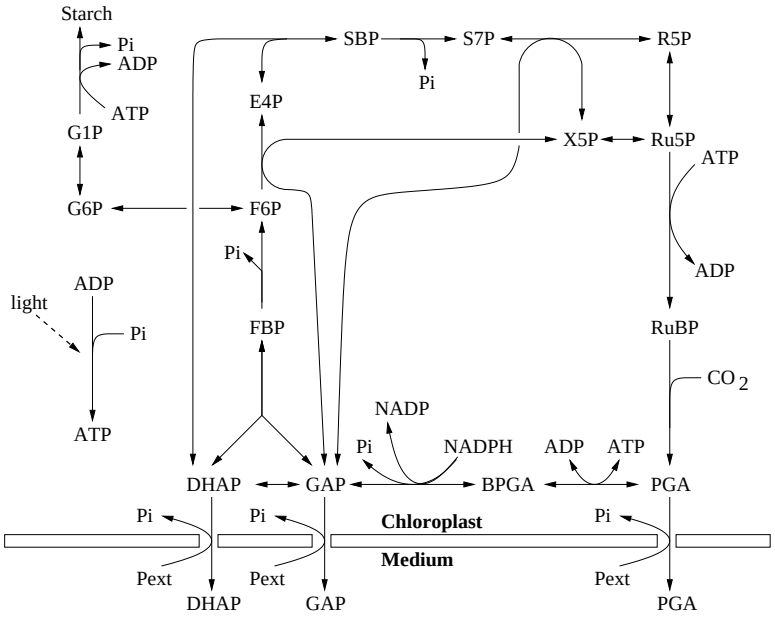

Metabolite abbreviations are as follows: phosphoglycerate (PGA), Bisphosphoglycerate (BPGA), glyceraldehyde phosphate (GAP), dihydroxyacetone phosphate (DHAP), fructose 1,6-bisphosphate (FBP), fructose 6-phosphate (F6P), glucose 6-phosphate (G6P), glucose 1-phosphate (G1P), erythrose 4-phosphate (E4P), sedoheptulose 1,7-bisphosphate (SBP), sedoheptulose 7-phosphate (S7P), xylulose 5-phosphate (X5P), ribose 5-phosphate (R5P), ribulose 5-phosphate (Ru5P), ribulose 1,5-bisphosphate (RuBP), inorganic phosphate (Pi).

In this section, we focus on an analysis of the model at a specific operating point, corresponding to the case investigated with previous kinetic models and describing the pathway under conditions of light and CO_2 saturation. All metabolite concentrations are as reported in refs (3) and (10) (in [mM]).

PGA	BPGA	GAP	DHAP	FBP	F6P	E4P	SBP	S7P	X5P
0.59	0.001	0.01	0.27	0.024	1.36	0.04	0.13	0.22	0.04

,

and (in [mM])

R5P	Ru5P	RuBP	G6P	G1P	ATP	ADP	P
0.06	0.02	0.14	3.12	0.18	0.39	0.11	8.1

.

The system is characterized by four independent steady-state fluxes, chosen here as the main export fluxes (in [mM $\cdot$ min^{-1}]).

ν_{starch}	ν_{PGA}	ν_{GAP}	ν_{DHAP}
0.16	7.1	0.56	12.0

.

Analysis of the Structural Kinetic Model

The experimentally observed operating point is stable for most realizations of the Jacobian. Fig. 15 shows the percentage of stable models with respect to ensemble size (number of realizations). As we are mostly interested in typical realizations, the percentage of stable models converges rather fast, despite the large number of parameters.

Similar to the glycolytic pathway, we examine the impact of individual reaction steps upon the stability of the system. Or rather, vice versa, we ask whether there are specific values of saturation parameters that would make the system prone to instability. Fig. 16 shows such a scenario, together with the unrestricted distribution of the largest real part within the spectrum of eigenvalues.
Since most models have $\lambda_R^{\max} < 0$, we compare the distribution of saturation parameters for models with $\lambda_R^{\max} > 0$ with the initial distribution. Marked changes are found for the triosephosphate isomerase (TBI: GAP $\leftrightarrow$ DHAP) with respect to GAP and for the G3P dehydrogenase (G3Pdh: BPGA+ NADPH $\leftrightarrow$ GAP + NADP + Pi) with respect to BPGA, see Fig. 17. In both cases high saturation (θ_x^μ small) leads to instability, as is verified in Fig. 16. Note that both reactions are not saturated in the original model, thus avoiding the instability.

The Matlab Code

```
function [J,Jx,CS,CJ] = CalvinCycle(t,p);
% The (schematic) function returns the normalized Jacobian
% of the model depicted in Fig. 6 of the manuscript.
% Note that this is a schematic function and
% not optimized for computational performance.



% The stoichiometric matrix
N = [ 2 -1  0  0  0  0  0  0  0  0  0  0  0  0  0  0 -1  0  0;
      0  1 -1  0  0  0  0  0  0  0  0  0  0  0  0  0  0  0  0;
      0  0  1 -1 -1  0 -1  0  0 -1  0  0  0  0  0  0  0  0 -1  0;
      0  0  0  1 -1  0  0 -1  0  0  0  0  0  0  0  0  0  0  0 -1;
      0  0  0  0  1 -1  0  0  0  0  0  0  0  0  0  0  0  0  0  0;
      0  0  0  0  0  1 -1  0  0  0  0  0  0 -1  0  0  0  0  0  0;
      0  0  0  0  0  0  1 -1  0  0  0  0  0  0  0  0  0  0  0  0;
      0  0  0  0  0  0  0  1 -1  0  0  0  0  0  0  0  0  0  0  0;
      0  0  0  0  0  0  0  0  1 -1  0  0  0  0  0  0  0  0  0  0;
      0  0  0  0  0  0  1  0  0  1  0 -1  0  0  0  0  0  0  0  0;
      0  0  0  0  0  0  0  0  0  1 -1  0  0  0  0  0  0  0  0  0;
      0  0  0  0  0  0  0  0  0  0  1  1 -1  0  0  0  0  0  0  0;
     -1  0  0  0  0  0  0  0  0  0  0  0  1  0  0  0  0  0  0  0;
      0  0  0  0  0  0  0  0  0  0  0  0  0  1 -1  0  0  0  0  0;
      0  0  0  0  0  0  0  0  0  0  0  0  0  0  1 -1  0  0  0  0;
      0 -1  0  0  0  0  0  0  0  0  0  0 -1  0  0 -1  1  0  0  0;
      0  1  0  0  0  0  0  0  0  0  0  0  1  0  0  1 -1  0  0  0;
      0  0  1  0  0  1  0  0  1  0  0  0  0  0  0  2 -1  1  1  1 ];



% The Null Space K
K = [6     3     3     3;
    12     5     6     6;
    12     5     6     6;
     5     2     2     3;
     3     1     1     1;
     3     1     1     1;
     2     1     1     1;
     2     1     1     1;
     2     1     1     1;
     2     1     1     1;
     2     1     1     1;
     4     2     2     2;
     6     3     3     3;
     1     0     0     0;
     1     0     0     0;
     1     0     0     0;
    19     8     9     9;
     0     1     0     0;
     0     0     1     0;
     0     0     0     1];
```

```
% DEFINE OPERATING POINT
% flux values
c1 = 0.289;
c2 = 12.74;
c3 = 1.0;
c4 = 21.6;
A = [c1 c2 c3 c4]';

A = A*1000/1800; % to obtain units in [mM/min]
V=K*A;           % the vector of steady state fluxes

% Define Concentrations (in [mM])
PGA = 0.59;
BPGA = 0.001;
GAP = 0.01;
DHAP = 0.27;
FBP = 0.024;
F6P = 1.36;
G6P = 3.12;
G1P = 0.18;
SBP = 0.13;
S7P = 0.22;
E4P = 0.04;
X5P = 0.04;
R5P = 0.06;
Ru5P = 0.02;
RuBP = 0.14;
P = 8.1;
ATP = 0.39;
ADP = 0.5-0.39;

X0 = [PGA BPGA GAP DHAP FBP F6P E4P SBP S7P X5P R5P Ru5P RuBP G6P G1P ATP ADP P ];

% Define Matrix of Saturation parameter
t;  % vector of substrate saturation (28 parameters)
p;  % global product inhibition

theta = [ -p    0    0    0    0    0    0    0    0    0    0    0  t(1)   0    0    0    0    0;
         t(2)  -p    0    0    0    0    0    0    0    0    0    0    0    0    0  t(3)  -p    0;
           0  t(4)  -p    0    0    0    0    0    0    0    0    0    0    0    0    0    0   -p;
           0    0  t(5)  -p    0    0    0    0    0    0    0    0    0    0    0    0    0    0;
           0    0  t(6) t(7)  -p    0    0    0    0    0    0    0    0    0    0    0    0    0;
           0    0    0    0  t(8)  -p    0    0    0    0    0    0    0    0    0    0    0   -p;
           0    0  t(9)   0    0 t(10)  -p    0    0   -p    0    0    0    0    0    0    0    0;
           0    0    0  t(11)  0    0 t(12)  -p    0    0    0    0    0    0    0    0    0    0;
           0    0    0    0    0    0    0 t(13)  -p    0    0    0    0    0    0    0    0   -p;
           0    0 t(14)   0    0    0    0    0 t(15)  -p   -p    0    0    0    0    0    0    0;
           0    0    0    0    0    0    0    0    0    0 t(16)  -p    0    0    0    0    0    0;
           0    0    0    0    0    0    0    0    0 t(17)   0   -p    0    0    0    0    0    0;
           0    0    0    0    0    0    0    0    0    0    0 t(18)  -p    0    0 t(19)  -p    0;
           0    0    0    0    0 t(20)   0    0    0    0    0    0    0   -p    0    0    0    0;
           0    0    0    0    0    0    0    0    0    0    0    0    0 t(21)  -p    0    0    0;
           0    0    0    0    0    0    0    0    0    0    0    0    0    0 t(22) t(23) -p   -p;
           0    0    0    0    0    0    0    0    0    0    0    0    0    0    0    0 t(24) t(25);
         t(26)  0    0    0    0    0    0    0    0    0    0    0    0    0    0    0    0   -p;
           0    0 t(27)   0    0    0    0    0    0    0    0    0    0    0    0    0    0   -p;
           0    0    0  t(28)  0    0    0    0    0    0    0    0    0    0    0    0    0   -p ];
```

```
% The reduced stoichiometric matrix, omitting ADP and P (mass conservation)
NN=N(1:16,:);

% The Link matrix, such that N = L*NN;
L=[diag(ones(16,1)) ;
   0   0   0  0   0  0  0  0  0  0  0  0  0  0  0 -1;
  -1 -2 -1 -1 -2 -1 -1 -2 -1 -1 -1 -1 -2 -1 -1 -1];



% TAKE MASS CONSERVATION INTO ACCOUNT
% 1) ADP + ATP = const
%    replace partial derivatives
dmdxR=dmdx(:,1:16);
LL = L(17,:).*X0(1:16)/ADP;
ix = find(dmdx(:,17)~=0);
for i=1:length(ix);
    dmdxR(ix(i),:) = dmdxR(ix(i),:) + LL*dmdx(ix(i),17);
end;

% 2) Pi = sum S_i
%    replace using the link matrix
LL = L(18,:).*X0(1:16)/P;
ix = find(dmdx(:,18)~=0);
for i=1:length(ix);
    dmdxR(ix(i),:) = dmdxR(ix(i),:) + LL*dmdx(ix(i),18);
end;


% DEFINE JACOBIAN
  V = V';
  X0 = X0';
  LAMBDA = NN.*V(ones(16,1),:);
  LAMBDA = LAMBDA./X0(1:16,ones(20,1));

J=LAMBDA*dmdxR;

% convert into original variables if needed
Jx=J;
for i=1:16; Jx(i,:)=Jx(i,:)*X0(i);end
for i=1:16; Jx(:,i)=Jx(:,i)/X0(i);end

% Control Coefficients
CS = -L*(JJx^(-1)*NN);

% Flux Control Coefficients
AA = V(ones(18,1),:)'./X0(1:18,ones(20,1))';
CJ = diag(ones(20,1))+(AA.*dmdx)*CS;
```

References

1. Heinrich, R. & Schuster, S. (1996) *The Regulation of Cellular Systems* (Chapman & Hall, New York).
2. Rohwer, J. M. & Botha, F. C. (2001) *Biochem. J.*, **358**, 437–445.
3. Petterson, G. & Ryde-Petterson, U. (1988) *Eur. J. Biochem.* **175**, 661–672.
4. Wolf, J., Passarge, J., Somsen, O. J. G., Snoep, J. L., Heinrich, R. & Westerhoff, H. V. (2000) *Biophys. J.* **78**, 1145–1153.
5. Bier, M., Bakker, B. M. & Westerhoff, H. V. (2000) *Biophys. J.* **78**, 1087–1093.
6. Gross, T. (2004) *Population Dynamics: General Results from Local Analysis* (Der Andere Verlag Tönning, Germany).
7. Kuznetsov, Yu. A. (1995) *Elements of Applied Bifurcation Theory* (Springer, Berlin).
8. Nielsen, K., Sørensen, P. G., Hynne, F. & Busse, H. G. (1998) *Biophys. Chem.* **72**, 49–62.
9. Hynne, F., Danø, S. & Sørensen, P. G. (2001) *Biophys. Chem.* **94**, 121–163.
10. Poolman, M. G., Fell, D. A. & Thomas, S. (2000) *J. Exp. Bot.* **51** (GMP Special issue), 319–328.